

# THE WEAK CARBON MONOXIDE EMISSION IN AN EXTREMELY METAL POOR GALAXY, SEXTANS A \*

YONG SHI<sup>1,2,3</sup>, JUNZHI WANG<sup>4,5</sup>, ZHI-YU ZHANG<sup>6</sup>, YU GAO<sup>7,5,3</sup>, LEE ARMUS<sup>8</sup>, GEORGE HELOU<sup>8</sup>, QIUSHENG GU<sup>1,2,3</sup>,  
SABRINA STIERWALT<sup>9</sup>

*Draft version August 9, 2018*

## ABSTRACT

Carbon monoxide (CO) is one of the primary coolants of gas and an easily accessible tracer of molecular gas in spiral galaxies but it is unclear if CO plays a similar role in metal poor dwarfs. We carried out a deep observation with IRAM 30 m to search for CO emission by targeting the brightest far-IR peak in a nearby extremely metal poor galaxy, Sextans A, with 7% Solar metallicity. A weak CO  $J=1-0$  emission is seen, which is already faint enough to place a strong constraint on the conversion factor ( $\alpha_{\text{CO}}$ ) from the CO luminosity to the molecular gas mass that is derived from the spatially resolved dust mass map. The  $\alpha_{\text{CO}}$  is at least seven hundred times the Milky Way value. This indicates that CO emission is exceedingly weak in extremely metal poor galaxies, challenging its role as a coolant in these galaxies.

*Subject headings:* galaxies: dwarf – submillimeter: ISM – galaxies: ISM

## 1. INTRODUCTION

Stars form out of molecular clouds (Kennicutt 1998; Gao & Solomon 2004). The efficient cooling of molecular gas is the prerequisite for gas collapse and star formation. Among molecular species, carbon monoxide (CO) plays an important role in cooling molecular gas in the low temperature and density regime (Goldsmith 2001). The CO emission is thus related to the fundamental question about how stars form out of gas. CO cools gas by radiation, and its bright emission renders CO the most common tracer of the molecular gas mass (Young & Scoville 1982), while the two most abundant components, H<sub>2</sub> and He, cannot be observed directly in emission at the characteristic temperature of molecular gas clouds. Over the past decade, the CO emission has been detected in galaxies with increasingly lower metallicity (Israel 1997; Taylor et al. 1998; Leroy et al. 2007, 2011), down to 15% Solar (Elmegreen et al. 2013). The conversion factor from CO to H<sub>2</sub> (referred as  $\alpha_{\text{CO}}$ ) has been constrained by comparing with the molecular gas mass inferred from other methods, showing values 10-100 times larger than the Milky Way value (Bolatto et al.

2013) in low metallicity environments. Probing CO emission at lower metallicities establishes if CO emission can be an efficient gas coolant and effective tracer of molecular gas in metal poor galaxies both locally and in early Universe.

Sextans A is a dwarf irregular at 1.4 Mpc with oxygen abundance of 7% Solar (Pettini & Pagel 2004; Kniazev et al. 2005). Its proximity increases the detectability of potential CO emission in the galaxy. It is one of a few extremely metal poor galaxies whose molecular gas masses have been estimated through the spatially resolved dust map (Shi et al. 2014), arguably the most accessible way for cold gas mass measurements in metal poor galaxies (Bolatto et al. 2013). The data are presented in § 2. The result and discussion are in § 3 and § 4, respectively. Conclusions are in § 5.

## 2. OBSERVATIONS

The CO  $J=1-0$  observations towards the star formation region (RA: 10:11:06.55, DEC: -04:42:04.70, J2000) in Sextans A were done from Aug. 23th to Aug 25th 2014, using the IRAM 30 meter millimeter telescope at Pico Veleta, Spain. The target region, which is 22 arcsec as the IRAM beam size at this frequency, is the far-IR peak as shown in Fig. 1. The Eight Mixer Receiver (EMIR) with dual-polarization and the Fourier Transform Spectrometers (FTS) backend were used, which gave the frequency channel spacing of 195 KHz. The standard wobbler switching mode with a  $\pm 120''$  offset at 0.5 Hz beam throwing was used for the observations. Pointing and focusing were checked about every 2 hours with nearby strong millimeter emitting quasi-stellar objects. We read out the spectra every 2 minutes, while the typical system temperature ( $T_{\text{sys}}$ ) was about 280 K at this band. Data reduction was conducted with the CLASS in GILDAS software package. We checked each spectrum and only used the spectra with  $T_{\text{sys}}$  less than 280 K for final discussion. After throwing out about 50% spectra, the total on source time was about 5 hours, which gave the noise level of about 4.1 mK in main beam temperature after smoothing the frequency resolution to 6.2 MHz ( $\sim 16 \text{ km s}^{-1}$ ).

\*BASED ON OBSERVATIONS CARRIED OUT WITH THE IRAM 30M TELESCOPE. IRAM IS SUPPORTED BY INSU/CNRS (FRANCE), MPG (GERMANY) AND IGN (SPAIN).

Electronic address: yshipku@gmail.com

<sup>1</sup> School of Astronomy and Space Science, Nanjing University, Nanjing 210093, China.

<sup>2</sup> Key Laboratory of Modern Astronomy and Astrophysics (Nanjing University), Ministry of Education, Nanjing 210093, China.

<sup>3</sup> Collaborative Innovation Center of Modern Astronomy and Space Exploration, Nanjing 210093, China.

<sup>4</sup> Shanghai Astronomical Observatory, Chinese Academy of Sciences, 80 Nandan Road, Shanghai 200030, China.

<sup>5</sup> Key Laboratory for Radio Astronomy, Chinese Academy of Sciences.

<sup>6</sup> Institute for Astronomy, University of Edinburgh, Royal Observatory, Blackford Hill, Edinburgh EH9 3HJ, UK

<sup>7</sup> Purple Mountain Observatory, Chinese Academy of Sciences, 2 West Beijing Road, Nanjing 210008, China.

<sup>8</sup> Infrared Processing and Analysis Center, California Institute of Technology, 1200 E. California Blvd, Pasadena, CA 91125, USA.

<sup>9</sup> Department of Astronomy, University of Virginia, P.O. Box 400325, Charlottesville, VA 22904, USA.

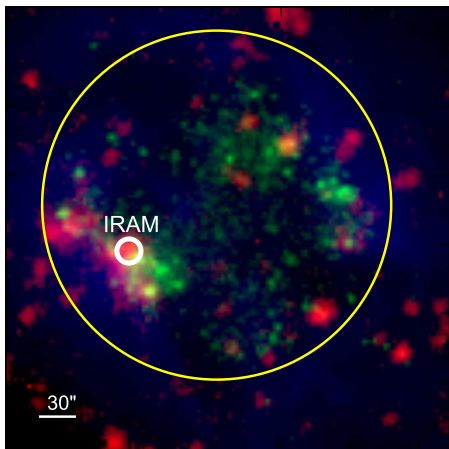


FIG. 1.— False-color, multi-wavelength images of Sextans A. Red is the sum of *Herschel* 160 and 250  $\mu\text{m}$  data, green is GALEX far-UV, and blue is radio 21 cm data showing the HI atomic gas. The IRAM 30 m pointing at CO  $J=1-0$  with the beam size is indicated by the white circle, while the yellow circle indicates the star-forming disk defined at a surface brightness of 25.9 ABmag arcsec $^{-2}$  in the GALEX far-UV band.

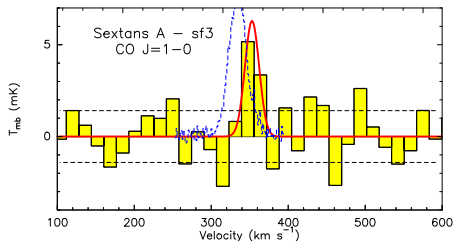


FIG. 2.— The submm spectrum around the CO  $J=1-0$  frequency with source redshift  $cz=324$  km/s. The red Gaussian profile is the fit to the signal at 350 km/s, which gives signal-to-noise ratio of 3.7 for the integrated flux. The two black dotted lines are the  $1-\sigma$  noise levels. The blue curve indicates the velocity of the HI emission line within the IRAM beam as measured from the HI data but with the absolute intensity scaled arbitrary (Ott et al. 2012).

The *Herschel* data at 70, 160, 250 and 350  $\mu\text{m}$ , and the *Spitzer* data at 3.6, 4.5, 5.6, 8.0 and 24  $\mu\text{m}$  data are from Shi et al. (2014) and Dale et al. (2009), respectively. Because the dust emission within the IRAM beam is partially resolved instead of a simple point spread function, to measure the photometry within the IRAM beam, we first convolved all images to the 350  $\mu\text{m}$  resolution based on the convolution Kernels (Aniano et al. 2011). Aperture photometry at all bands were then measured at this spatial resolution. The corresponding aperture correction factor is taken as the ratio of the 70  $\mu\text{m}$  photometry at its native resolution to that at the 350  $\mu\text{m}$  resolution by assuming that the 70  $\mu\text{m}$  map at its native resolution can resolve the dust structure. We further included the far-ultraviolet (UV) images from the *GALEX* Space Telescope archive as well as maps of atomic gas (Ott et al. 2012).

### 3. RESULTS

Fig. 2 shows the observed CO  $J=1-0$  spectrum at a resolution of 16 km/s with  $cz=324$  km/s. A marginal signal at 350 km/s was seen. A Gaussian fitting gives S/N of 3.7 for the integrated flux, a width of  $21\pm 12$  km/s and peak intensity of 6.3 mK while the  $1-\sigma$  noise is 1.4 mK. The distribution of the noise level is slightly non-Gaussian. Using the negative values of channels over a velocity range from -500 to 1500 km/s, we estimated a

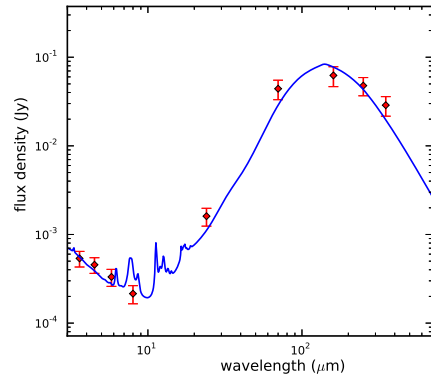


FIG. 3.— The Infrared SED of Sextans A within the IRAM beam is fitted to derive the dust mass. Red symbols are the *Spitzer* and *Herschel* photometric points with  $1-\sigma$  error bars. The blue solid line indicates the best-fit by the dust model (Draine & Li 2007).

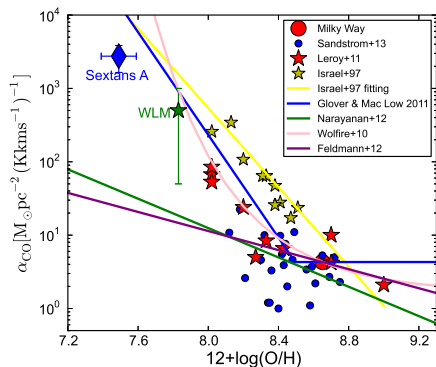


FIG. 4.— The conversion factor ( $\alpha_{\text{CO}}$ ) from the CO luminosity to the molecular gas mass for Sextans A is compared to those at higher metallicities. Symbols are observations in the literature (Israel 1997; Leroy et al. 2011; Sandstrom et al. 2013; Elmegreen et al. 2013) where molecular gas masses are all based on the spatially resolved dust maps except for WLM (see text for the detail). Lines are models, either empirical (Israel 1997), or theoretical models (Wolfire et al. 2010; Glover & Mac Low 2011; Narayanan et al. 2012; Feldmann et al. 2012).

probability of 0.05% for the signal to be artificial, which corresponds to a  $3.4 \sigma$  significance for a Gaussian distribution of noises. The feature lies within the velocity range of atomic gas as shown in Fig. 2. The offset in the velocity between the two lines may be reasonable as the two trace different phases of ISM. As listed in Table 1, the intensity  $I_{\text{CO}(J=1-0)}$  is  $145\pm 39$  mK km s $^{-1}$  in  $T_{\text{mb}}$ , corresponding to a point source luminosity (Gao & Solomon 2004) of  $\sim (3.7\pm 1.0)\times 10^3$  K km s $^{-1}$  pc $^2$  for a beam size of 22 arcsec, much smaller than the previous upperlimits (Taylor et al. 1998) of a few  $\times 10^4$  K km s $^{-1}$  pc $^2$  observed at the position (RA=10h11m07.3s, dec=-4d42m22.5s, J2000) near our pointing with a beam size of 55 arcsec. The  $3-\sigma$  CO  $J=2-1$  assuming the same velocity dispersion as CO  $J=1-0$  is 460 mK km/s.

The conversion factor  $\alpha_{\text{CO}}$  from CO to  $\text{H}_2$  is quantified by comparing the CO luminosity to the molecular gas mass that is inferred from the spatially resolved dust map (Israel 1997; Leroy et al. 2011; Sandstrom et al. 2013). As shown in Fig. 3, the infrared SED is first fitted with the model of Draine & Li (2007) as detailed in Shi et al. (2014), based on which the total cold gas (HI+ $\text{H}_2$ ) within the IRAM beam is measured by multiplying the dust mass with the gas-to-dust ratio derived from the diffuse

TABLE 1  
THE PROPERTIES OF THE DWARF GALAXY SEXTANS A WITH THE IRAM CO (1-0) BEAM.

$I_{\text{CO}(J=1-0)}$ mK km/s	$I_{\text{CO}(J=2-1)}$ mK km/s	$L_{\text{CO}(J=1-0)}$ K km/s pc <sup>2</sup>	$M_{\text{dust}}$ M <sub>⊙</sub>	$M_{\text{H}_2+\text{HI}}^{\text{dust}}$ 10 <sup>7</sup> M <sub>⊙</sub>	$M_{\text{H}_2}^{\text{dust}}$ 10 <sup>7</sup> M <sub>⊙</sub>	$\alpha_{\text{CO}(J=1-0)}$ M <sub>⊙</sub> /pc <sup>2</sup> /(K km/s)	SFR 10 <sup>-4</sup> M <sub>⊙</sub> /yr	$L_{8-1000\mu\text{m}}$ 10 <sup>5</sup> L <sub>⊙</sub>	$M_{\text{star}}$ 10 <sup>5</sup> M <sub>⊙</sub>
145±39	< 460	3670±990	771±184	1.1±0.3	1.0±0.3	2750±1110	2.2±0.4	1.7±0.4	1.7±0.4

regions of the galaxy. As discussed in Shi et al. (2014), the derived total cold gas mass is not sensitive to the absolute dust mass but to the ratio of dust masses of star-forming and diffuse regions. As a result, as long as diffuse and star-forming regions have similar dust grains, different dust models gives a similar estimate of cold gas masses within the IRAM beam. To derive the gas mass of star-forming regions, we do assume star-forming regions have the same gas-to-dust ratio as the diffuse regions, which is true for spiral galaxies (e.g. Sandstrom et al. 2013). However, this assumption may break down in dwarfs as their star formation history is stochastic in both space and time so that both diffuse and star-forming regions are affected by different physical processes that impact the gas-to-dust ratio. For example, the SN shocks may continuously destroy the dust in the diffuse regions in the past yet meanwhile dust grains in dense clouds are protected from such destruction but instead grow further. Nevertheless, such a hypothesis needs systematic investigations before any conclusion can be made.

After subtracting the atomic gas mass from the derived total gas mass, the molecular gas mass is shown to be about 10<sup>7</sup> M<sub>⊙</sub> as listed in Table 1. The derived  $\alpha_{\text{CO}}$  value is about  $(2.8 \pm 1.1) \times 10^3 \text{ M}_{\odot} \text{ pc}^{-2} (\text{K km s}^{-1})^{-1}$ ,  $\sim 700$  times larger than the Milky Way value ( $4.3 \text{ M}_{\odot} \text{ pc}^{-2} (\text{K km s}^{-1})^{-1}$ ) (Bolatto et al. 2013). In Fig. 4, we compared our measurement to those in the literature (Israel 1997; Leroy et al. 2011; Sandstrom et al. 2013) whose molecular gas masses are derived in the same way as ours except for the galaxy Wolf-Lundmark-Melotte (WLM, Elmegreen et al. 2013). The gas-to-dust ratio used to derive the  $\alpha_{\text{CO}}$  of WLM is based on the relationship between  $\alpha_{\text{CO}}$  and metallicity (Rémy-Ruyer et al. 2014), which shows a large scatter ( $> 10$ ) around the metallicity of WLM. The metallicity measurement of Sextans A was not taken exactly at the CO pointing. But as no metallicity gradient is seen in Sextans A (Kniazev et al. 2005), we did not expect large offsets ( $> 0.1$  dex) from the value quoted here. Our  $\alpha_{\text{CO}}$  is much larger than those at higher metallicities. The overall trend of  $\alpha_{\text{CO}}$  with metallicity is very steep, with a power law index between 2.5 and 3. This implies that CO emission is very weak in extremely metal poor galaxies. While our works offer very interesting constraints on the  $\alpha_{\text{CO}}$  at extreme low metallicity, the result is solely based on one region of  $\sim 20$  arcsec compared to the entire galaxy of five arcmin. Only about 10% of the total molecular gas of Sextans A (Shi et al. 2014) is within the beam. Large scatters of  $\alpha_{\text{CO}}$  may be expected with future detections of CO emission over different regions of the galaxy.

The relative strength of the CO brightness can also be compared to other quantities of Sextans A measured within the IRAM beam as listed in Table 1. By integrating the IR SED of the IRAM region, the 8-1000  $\mu\text{m}$  infrared luminosity of dust within the beam is mea-

sured to be  $1.7 \times 10^5 L_{\odot}$ . So the CO luminosity in K km s<sup>-1</sup> pc<sup>2</sup> relative to the infrared luminosity in  $L_{\odot}$  is about 1:45, which is slightly larger than spiral galaxies (Genzel et al. 2010). This is partly caused by the rarity of both dust and CO in extremely metal poor galaxies while different excitation mechanisms for CO and dust must also play some roles. If comparing to the star formation rate (SFR) as measured from the far-UV luminosity (Kennicutt 1998), the SFR per CO luminosity is about ten times higher than star-forming non-merger massive galaxies (Genzel et al. 2010). If scaling by the stellar mass as measured from Spitzer 3.6 and 4.5  $\mu\text{m}$  measurements (Eskew et al. 2012), the CO luminosity per stellar mass of Sextans A within the IRAM beam is on average 10 times lower than non-merger massive galaxies (Genzel et al. 2010).

#### 4. DISCUSSIONS

The detection of CO  $J$  1-0 emission in Sextans A, if it is real, offers a crucial evidence for the existence of molecular gas in such a low metallicity environment, confirming the result inferred from the dust measurement (Shi et al. 2014). Although warm H<sub>2</sub> has been revealed by infrared spectroscopic observations in several extremely metal poor galaxies (Hunt et al. 2010), CO emission, unlike warm H<sub>2</sub> that traces shocked regions, is known as tracers of ISM where stars form in massive metal rich galaxies. The detection of CO in Sextans A is a first step toward determining whether CO can serve a similar role in extremely metal poor galaxies.

CO is one of few efficient coolants of molecular gas in galaxies. In extremely metal poor galaxies, due to the photo-dissociation, the CO can only survive in a tiny core of molecular gas clouds, while H<sub>2</sub> can be self-shielded and exist in thick envelopes surrounding the CO molecular core. Thus cooling through CO in extremely metal poor galaxies may be not as effective as in metal rich galaxies. If the CO molecular cores in metal poor galaxies follow the same relationship between the viral masses and CO luminosities of giant molecular clouds in Milky Way and nearby galaxies (Solomon et al. 1987; Bolatto et al. 2013), the viral mass of the CO molecule core for the observed CO luminosity is estimated to be about  $3 \times 10^4 \text{ M}_{\odot}$ . This is only a tiny fraction of dust-based total molecular gas mass, as small as 0.3%. Then the measured CO within the IRAM beam is associated with only a small fraction of the total molecular gas within the same beam, and it cannot effectively cool the bulk of the molecular gas in Sextans A. As a result of the photo-dissociation of CO, atomic or ionized carbon may become abundant. Studies did show that [CII] 158  $\mu\text{m}$  is much brighter relative to CO in dwarfs as compared to in spirals (Israel & Maloney 2011; Brauher et al. 2008; Madden et al. 2013). With spatially resolved studies of IC 10, Madden et al. (1997) showed that the H<sub>2</sub> column

density associated with ionized carbon can be five times the observed HI density in order to interpret the cooling as implied by the [CII] luminosity, and the associated H<sub>2</sub> mass may be 100 times the mass of H<sub>2</sub> associated with CO. However, unlike CO, [CII] with its high excitation temperature (97 K) still could not cool the gas to the low temperature at which gas may contract to the high density for stars to form.

Fig. 4 further shows the comparison between the measured extreme large  $\alpha_{\text{CO}}$  of Sextans A with models' predictions. The empirical relationship (yellow solid line, Israel 1997) based on galaxies above 20% $Z_{\odot}$  predicts that  $\alpha_{\text{CO}} \propto Z^{2.7}$ , giving a value several times larger than our observed one at 7% $Z_{\odot}$ . Based on the principle that the CO abundance is primarily regulated by photo-dissociation and the H<sub>2</sub> is self-shielded, theoretical models of Glover & Mac Low (2011) and Wolfire et al. (2010) predict that  $\alpha_{\text{CO}}$  is a strong function of the visual extinction for individual clouds. If assuming the visual extinction is proportional to the metallicity,  $\alpha_{\text{CO}}$  then increases rapidly with the decreasing metallicity in both models, predicting values larger than the observed for Sextans A as shown in Fig. 4. The model of Narayanan et al. (2012) also employed photo-dissociation region models but for the integrated galaxies instead of individual clouds, and found on average a flat trend of  $\alpha_{\text{CO}}$  as a function of metallicity, producing a value much smaller than the observed one at 7% $Z_{\odot}$ . Unlike the above models, the model of Feldmann et al. (2012) employs small scale magneto-hydrodynamic simulations combined with large-scale simulations of gas distributions to predict  $\alpha_{\text{CO}}$  as a function of metallicities. For physical scales of our IRAM beam size (sub-kpc), a shallow trend as indicated by the purple line in Fig. 4 is predicted, with predicted values significantly smaller than the observation.

As a summary, current models predict a large range of  $\alpha_{\text{CO}}$  at the metallicity of Sextans A, some significantly larger than the observed one while some much smaller

than the observation. It is still difficult to judge which model is better or worse just based on one data point, which is also because many assumptions are invoked in theoretical models in order to produce the trend of  $\alpha_{\text{CO}}$  as a function of metallicity. A large range of model's predictions reflects the limited knowledge about CO formation and destruction, as well as properties of gas clouds over different spatial scales at the extreme low metallicity. If  $\alpha_{\text{CO}}$  is truly large as seen in this study, CO may be not an efficient coolant in metal poor galaxies, and its application as a tracer of the molecular gas mass may be inappropriate in the early Universe.

## 5. CONCLUSIONS

We reported a marginal detection of CO  $J=1-0$  emission by targeting the brightest far-IR peak in an extremely metal poor galaxy, Sextans A. The signal is about 10 km/s offset from the HI peak within the same beam. The  $\alpha_{\text{CO}}$  is further derived by comparing the estimated CO flux to the H<sub>2</sub> mass as inferred from the dust map. In spite of a marginal signal, the observation is deep enough to play a strong limit on the  $\alpha_{\text{CO}}$  that is about seven hundred times the Milky Way value. This suggests that CO emission is exceedingly weak in extremely metal poor galaxies, challenging its role as a gas coolant in these galaxies. Current theoretical models produce a large range of  $\alpha_{\text{CO}}$  at the metallicity of Sextans A.

We thank the anonymous referee for constructive comments that improve the paper significantly. Y.S. acknowledges support for this work from Natural Science Foundation of China under the grant of 11373021 and by the Strategic Priority Research Program "The Emergence of Cosmological Structures" of the Chinese Academy of Sciences, Grant No. XDB09000000. Y.G. is supported under grants of 11390373, 11420101002 & XDB09000000.

## REFERENCES

- Aniano, G., Draine, B. T., Gordon, K. D., & Sandstrom, K. 2011, *PASP*, 123, 1218
- Bolatto, A. D., Wolfire, M., & Leroy, A. K. 2013, *ARA&A*, 51, 207
- Brauher, J. R., Dale, D. A., & Helou, G. 2008, *ApJS*, 178, 280
- Dale, D. A., Cohen, S. A., Johnson, L. C., et al. 2009, *ApJ*, 703, 517
- Draine, B. T., & Li, A. 2007, *ApJ*, 657, 810
- Elmegreen, B. G., Rubio, M., Hunter, D. A., et al. 2013, *Nature*, 495, 487
- Eskew, M., Zaritsky, D., & Meidt, S. 2012, *AJ*, 143, 139
- Feldmann, R., Gnedin, N. Y., & Kravtsov, A. V. 2012, *ApJ*, 747, 124
- Gao, Y., & Solomon, P. M. 2004, *ApJ*, 606, 271
- Genzel, R., Tacconi, L. J., Gracia-Carpio, J., et al. 2010, *MNRAS*, 407, 2091
- Glover, S. C. O., & Mac Low, M.-M. 2011, *MNRAS*, 412, 337
- Goldsmith, P. F. 2001, *ApJ*, 557, 736
- Hunt, L. K., Thuan, T. X., Izotov, Y. I., & Sauvage, M. 2010, *ApJ*, 712, 164
- Israel, F. P. 1997, *A&A*, 328, 471
- Israel, F. P., & Maloney, P. R. 2011, *A&A*, 531, AA19
- Kennicutt, R. C., Jr. 1998, *ApJ*, 498, 541
- Kennicutt, R. C., Jr. 1998, *ARA&A*, 36, 189
- Kniazev, A. Y., Grebel, E. K., Pustilnik, S. A., Pramskij, A. G., & Zucker, D. B. 2005, *AJ*, 130, 1558
- Leroy, A., Cannon, J., Walter, F., Bolatto, A., & Weiss, A. 2007, *ApJ*, 663, 990
- Leroy, A. K., Bolatto, A., Gordon, K., et al. 2011, *ApJ*, 737, 12
- Madden, S. C., Poglitsch, A., Geis, N., Stacey, G. J., & Townes, C. H. 1997, *ApJ*, 483, 200
- Madden, S. C., Rémy-Ruyer, A., Galametz, M., et al. 2013, *PASP*, 125, 600
- Narayanan, D., Krumholz, M. R., Ostriker, E. C., & Hernquist, L. 2012, *MNRAS*, 421, 3127
- Ott, J., Stilp, A. M., Warren, S. R., et al. 2012, *AJ*, 144, 123
- Pettini, M., & Pagel, B. E. J. 2004, *MNRAS*, 348, L59
- Rémy-Ruyer, A., Madden, S. C., Galliano, F., et al. 2014, *A&A*, 563, A31
- Sandstrom, K. M., Leroy, A. K., Walter, F., et al. 2013, *ApJ*, 777, 5
- Shi, Y., Armus, L., Helou, G., et al. 2014, *Nature*, 514, 335
- Solomon, P. M., Rivolo, A. R., Barrett, J., & Yahil, A. 1987, *ApJ*, 319, 730
- Taylor, C. L., Kobulnicky, H. A., & Skillman, E. D. 1998, *AJ*, 116, 2746
- Wolfire, M. G., Hollenbach, D., & McKee, C. F. 2010, *ApJ*, 716, 1191
- Young, J. S., & Scoville, N. 1982, *ApJ*, 258, 467